Solar Energy Materials & Solar Cells 140 (2015) 108–114

Contents lists available at ScienceDirect

Solar Energy Materials & Solar Cells

journal homepage: www.elsevier.com/locate/solmat

Iron pyrite nanocrystal film serves as a copper-free back contact for polycrystalline CdTe thin film solar cells

Khagendra P. Bhandari, Prakash Koirala, Naba R. Paudel, Rajendra R. Khanal, Adam B. Phillips, Yanfa Yan, Robert W. Collins, Michael J. Heben, Randy J. Ellingson *

Department of Physics and Astronomy, The University of Toledo, 2801 W. Bancroft Street, Toledo, OH 43606, USA

ARTICLE INFO

Article history:
Received 8 December 2014
Received in revised form
26 February 2015
Accepted 31 March 2015

Keywords:
Iron pyrite
Cadmium telluride
Back contact
Thin film
Solar cell
Nanocrystalline

ABSTRACT

We report the application of thin film nanocrystalline (NC) FeS_2 as the copper-free back contact for CdTe solar cells. The FeS_2-NC layer is prepared from solution directly on the CdTe surface using drop-casting coupled with a hydrazine treatment at ambient temperature and pressure, and requires no thermal treatment. Copper-free solar cells based on the CdS/CdTe/FeS_2-NC/Au architecture exhibit device efficiencies $>90\%$ that of a standard Cu/Au back contact devices. The FeS_2-NC back contact solar cells show good thermal stability under initial tests. Devices prepared with untreated FeS_2-NC back contacts display a strong "S-kink" behavior which we correlate with a high hole-transport barrier arising from inter-NC organic surfactant molecules.

1. Introduction

Following significant focus on FeS_2 solar cells in the early years of thin film photovoltaics (PV) [1–7], FeS_2 has in recent years attracted renewed attention as a potential light-absorbing layer in thin film PV cells based on its suitable band gap energy, high absorption coefficient, low toxicity, and elemental abundance [8–16]. However, FeS_2-based PV devices have thus far performed poorly compared with devices based on other recently-developed absorber materials (e.g. CZTS, perovskites such as methylammonium lead iodide, and PbS quantum dots) [17–21]. Tributsch et al.'s extensive efforts initiated in the 1980s led ultimately to a 2.8% efficient photo-electrochemical cell based on single crystal FeS_2 electrodes using an iodide/tri-iodide (I^-/I_3^-) redox couple [1–4]. This result stands as the efficiency record for FeS_2-based solar cells, owing in part to the well-recognized challenges presented by high defect densities resulting from poor phase and stoichiometry control [22,23] Specifically, phase purity has been an expressed concern for effective FeS_2 photovoltaic devices because the different iron sulfide phases of Fe_xS_y exhibit a wide range of optoelectronic properties [24].

Here we report on the discovery that the properties of FeS_2 nanocrystal (NC)-based thin films yield excellent performance as a low barrier back contact to CdS/CdTe solar cells, without copper pre-treatment of the CdTe p-type film. Cadmium telluride thin film modules represent ~7% of the 32 GW of PV modules produced in 2012, and CdTe manufacturing produces the lowest cost on a per-Watt basis ($0.49/$W_p$) [25]. The high work function of CdTe (~5.7 eV) [26,27] presents a long-studied challenge to creating a low-barrier, pseudo-ohmic back contact for use in the CdS/CdTe architecture [28]. Standard back contact preparation involves the introduction of copper, as a thin evaporated layer or through a $CuCl_2$ solution deposition, followed by thermal diffusion to produce a highly-doped near-contact CdTe layer that narrows the barrier at the interface with a metal, such as Au [29,30]. However, several studies have shown that Cu diffuses readily, and over time reaches and crosses the CdS/CdTe interface, reducing the operating voltage of the device [30,31]. Copper diffusion therefore serves as a degradation pathway, influencing device performance over the life of a PV system and ultimately degrading the economic performance of the technology [32].

As-deposited FeS_2-NC films studied at room-temperature using four-point probe and Hall measurements showed low resistivity (~100 Ω cm), high free carrier concentrations (~10^{19} cm^{-3}), and low mobility (~10^{-1} $cm^2\,V^{-1}\,s^{-1}$). In addition, FeS_2 NCs clearly show sub-bandgap optical absorption, indicating a significant density of sub-bandgap electronic states arising from core and/or surface defects. Consequently, these films are not expected to be effective absorber layers in photovoltaic devices. Indeed, the highest

* Corresponding author. Tel.: +1 419 530 3874.
E-mail address: randy.ellingson@utoledo.edu (R.J. Ellingson).

http://dx.doi.org/10.1016/j.solmat.2015.03.032
0927-0248/

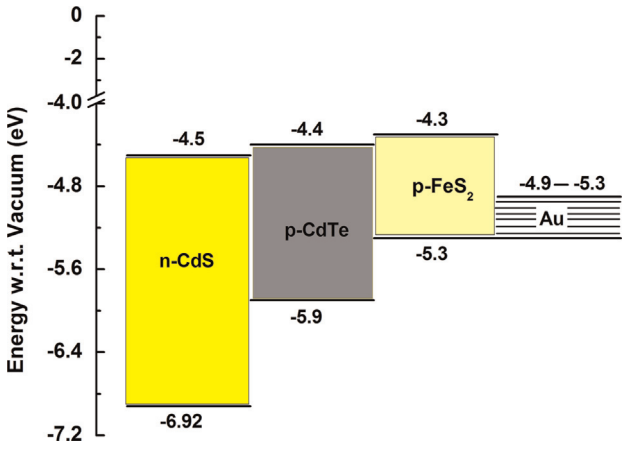

Fig. 1. Non-interacting band diagram showing conduction and valence band positions relative to the vacuum level.

open circuit voltage (V_{OC}) attained in Tributsch's work was ~0.28 V, much lower than the theoretically attainable value of ~0.5 V [33]; the authors attributed the low photovoltage to both strong Fermi level pinning associated with surface states and to bulk defects caused by sulfur deficiency [34]. For purposes of comparison, note that CdTe, which has achieved a conversion efficiency of 21.5% under standard test conditions [35], typically exhibits a resistivity of ~10^4 Ω cm, a free carrier concentration of ~10^{14} cm^{-3}, and a hole mobility of ~10^2 cm^2 V^{-1} s [36,37].

Although FeS_2 has not served well as a solar cell absorber layer, the high free carrier concentration and low resistivity observed in our FeS_2-NC films suggest promise as a conductive low barrier contact to CdTe. The work function of FeS_2 ($\varphi \approx 5.0$ eV [4], 5.45 eV [38]) compares favorably with that of Au ($\varphi \approx 4.9$–5.3 eV) [39–41] and indicates the possibility of a barrier-less or low-barrier interface at the CdTe/FeS_2 junction. As shown in Fig. 1, the non-interacting band diagram [10,42,43] indicates the possibility of a low-barrier interface at the CdTe/FeS_2 junction. For CdS/CdTe solar cells, conventional back contacts are commonly made with Cu/Au or Cu/graphite [44]. Graphene was employed as a back contact for thin film CdTe solar cells, but to narrow the barrier at the CdTe/graphene interface, either Cu or B was incorporated [45,46]. Phillips et al. recently reported that thin films of single wall carbon nanotubes (SWNTs) make stable, high-performance back contacts to CdTe without introduction of Cu [47]. Their analysis suggests that semiconducting SWNTs make ohmic contacts with p-CdTe while metallic SWNTs make rectifying contacts to p-CdTe. Our initial results applying FeS_2 NCs as the back contact to CdTe solar cells show substantial promise for this Cu-free and potentially low-cost approach.

Solution-based synthesis and deposition offers a potentially low-cost and scalable photovoltaic manufacturing method for large glass substrate processes and roll-to-roll processing on flexible substrates. Numerous routes have been followed to synthesize FeS_2 NCs [8–10], and we follow a solution-based approach based on thermal injection reaction, in the presence of trioctylphosphine oxide (TOPO) or 1,2-hexanediol, of an iron salt solution with an elemental sulfur source. While others have utilized $FeCl_2$ as the iron source, we have found that $FeBr_2$ yields improved results regarding crystal structure and infrared absorption [48]. We prepared drop-cast FeS_2 NC films using a layer-by-layer (LbL) method [20,49–51] in a nitrogen environment, with and without a process consisting of layer treatment by dipping into 1 M hydrazine in ethanol. The hydrazine-treated LbL films were more conducting due to the removal of the long insulating capping ligands.

2. Experimental details

2.1. Synthesis of FeS_2 NCs

As described elsewhere [48], synthesis of iron pyrite nanocrystals is performed in a Schlenk line under N_2 environment. In a typical synthesis, about 0.49 mmol of $FeBr_2$ and 1 mmol of trioctylphosphine oxide (or 135 μL of 1,2-hexanediol) are mixed in 10 mL of oleylamine (OLA) in a three neck flask under constant stirring. The $FeBr_2$ mixture is heated to 170 °C for ~2.5 h using a heating mantle; during this time, the sulfur precursor solution is prepared by dissolving 3 mmol of elemental sulfur in 5 mL of OLA. After 2.5 h of heating at 170 °C, the temperature of the $FeBr_2$ solution is raised toward 220 °C, and once it exceeds 216 °C, the sulfur solution is rapidly injected. Following two hours stirring at 220 °C, the NC solution is allowed to cool to room temperature, with continued stirring. Nanocrystals so obtained are washed a minimum of three times using methanol as a non-solvent and toluene as solvent. Finally NCs so obtained are dried under nitrogen gas flow.

2.2. FeS_2 film fabrication

To fabricate FeS_2-NC films, we utilize a drop-cast method in a layer-by-layer (LbL) process. We prepare an FeS_2 NC solution in chloroform at a concentration of ~6 mg/ml, and proceed with film formation, in an N_2 environment, as follows. A layer of drop-cast NCs is deposited onto the chosen substrate, and allowed to dry. At this point, the film can optionally be treated with hydrazine for ligand removal (vide infra). In the case of an untreated film, the film thickness may be increased by simply repeating the drop-cast process followed by the drying process; preparation of a ~1 μm film typically requires 2 layers.

Preparation of an FeS_2-NC film treated with hydrazine to remove the surfactant is accomplished as follows. Subsequent to the first drop-cast layer deposition, the film is allowed to dry in the N_2 environment. The film is subsequently submerged in a 1 M hydrazine solution in ethanol for ~2 min. The film is withdrawn from the hydrazine solution and immediately submerged into a pure ethanol solution to remove any residual surfactant or hydrazine – i.e., as a rinse. The film is then allowed to dry. To attain a thicker film, the drop-cast/dry/hydrazine/rinse/dry process may be repeated as necessary.

2.3. CdS/CdTe device fabrication

The CdS and CdTe layers were deposited by RF magnetron sputtering, or by closed spaced sublimation (CSS), onto NSG TEC™15 TCO-coated glass (Pilkington N.A.), which consists of a dielectric film stack including SiO_2, SnO_2, and SnO_2:F deposited on soda lime glass [52]. As compared with sputtered CdS/CdTe films, CSS yields films with larger initial CdTe grain size (2–5 μm vs. 200–300 nm) due to the higher substrate temperature (~600 °C for CSS vs. ~275 °C for sputtered films) [53,54]. Following the CdTe deposition, a $CdCl_2$ treatment was carried out by applying a saturated solution of $CdCl_2$-methanol and subsequently annealing at 387 °C for 30 min in dry air to advance grain growth, release interfacial strain, and facilitate sulfur and tellurium mixing at the CdS/CdTe interface [55]. The thickness of CdS films in both methods was ~80 nm whereas the sputtered CdTe was ~2.0 μm and the CSS CdTe was ~4 μm. Our sputtered CdS/CdTe films enable best device efficiency of ~12%, and our CSS CdS/CdTe films enable best device efficiency of ~14.0%; all device efficiency measurements are made under AM1.5G simulated solar spectrum at ambient laboratory temperature. Following CdS/CdTe deposition, the standard back contact consists of a Cu/Au sequential deposition in which ~3 nm

of Cu followed by ~30 nm of Au is evaporated onto the CdTe, and the film is then heated to 150 °C for 45 min in air to drive Cu diffusion (Fig. S1, Supporting information). Similarly for FeS_2/Au back contact deposition, 30 nm Au is thermally evaporated onto FeS_2 NC film deposited at room temperature. The device area of 0.08 cm^2 is defined by using a shadow metal mask while depositing Cu/Au back contact. Since FeS_2 NC film is conductive, shadow mask cannot be used while making Au layer on top of NC film. In this case, FeS_2/Au or Cu/FeS_2/Au composite layers are scribed manually or using laser scriber to define an area equal to 0.085 cm^2.

3. Results and discussion

The cross-sectional SEM image shown in Fig. 2 was obtained for a CdS/CdTe device prepared in a stepwise process on TEC™15 glass using RF magnetron sputtering deposition of CdS (~80 nm) and CdTe (~2 μm), standard $CdCl_2$ treatment, LbL drop-cast deposition of NC FeS_2, and evaporation of ~30 nm Au for improved electrical contact for *J–V* and QE characterization. The treated and untreated films appear physically essentially indistinguishable in cross-sectional SEM as shown in Fig. S2. Current density/voltage (*J–V*) characteristics for best-performing sputtered CdTe devices prepared with different back contacts are shown in Fig. 3a, and average device parameters are presented in Table 1. These solar cells were prepared on 1″ × 1″ TEC™15-coated glass substrates.

Each sample set consists of multiple cells prepared on a single substrate, based on either shadow masking or scribing. Table 1 demonstrates average and standard deviations of 15 cells of each contact type. Each *J–V* curve in Fig. 3a represents a highest efficiency curve from among the 15 cells, with solid curves representing measurements under simulated AM1.5 illumination, and dashed curves represent device measurements in the dark. The red curve represents the *J–V* behavior when 30 nm Au was evaporated as a back contact, without any Cu diffusion layer. Although J_{SC} does not drop significantly compared to the other back contact types, V_{OC} and efficiency (η) are poor when Au alone is used as the CdTe contact. Because of CdTe's electron affinity (−4.4 eV) [56], a high work function material is required to form a low barrier height contact with p-type CdTe. To attain an ohmic junction with p-type CdTe, a metal should exhibit a minimum work function of ~5.9 eV [29]. Since no metals have a sufficiently high work function, any metal forms a Schottky junction with non-zero barrier height when contacting CdTe at its typical free hole concentration. Because the CdTe/Au Schottky junction opposes the main diode

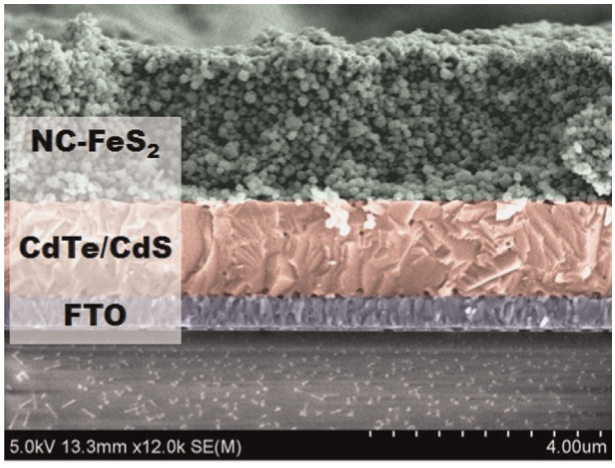

Fig. 2. Cross-sectional SEM image, obtained by secondary electron detector, of drop-cast hydrazine-treated FeS_2-NC thin film contact formed on a sputtered CdS/CdTe thin film.

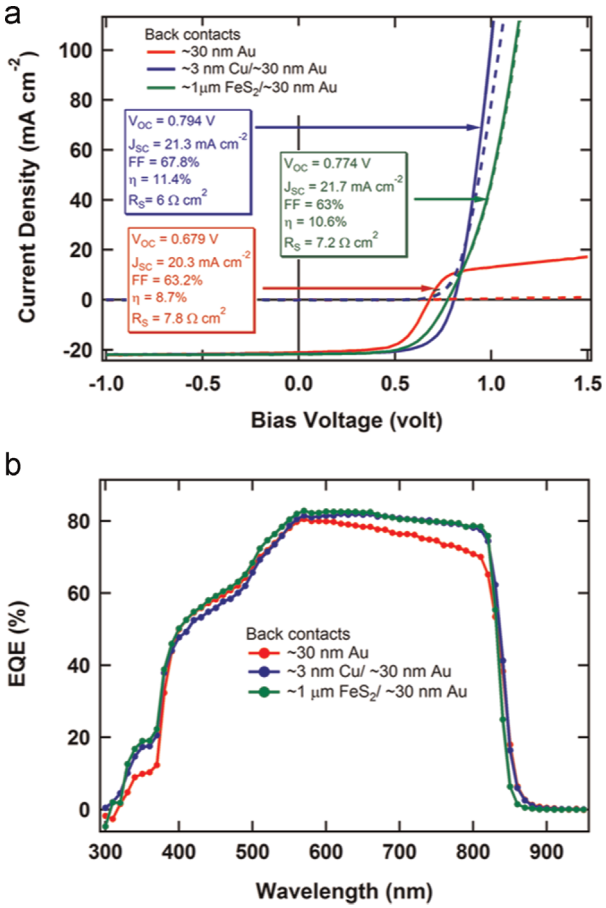

Fig. 3. (a) Current density vs. bias voltage measurements of sputtered CdTe device with Au, Cu/Au, and FeS_2-NC/Au back contacts obtained under simulated AM1.5G solar spectrum, (b) external quantum efficiency for CdTe devices with Au, Cu/Au and FeS_2-NC/Au back contacts. (For interpretation of the references to color in this figure, the reader is referred to the web version of this article.)

formed at the CdS/CdTe interface [57], hole transport is limited at the back contact. The current–voltage curve "rolls over" at forward bias, decreasing both the fill factor and the open-circuit voltage [58]. The problem associated with using a metal-only (e.g. Au) back contact is alleviated by depositing ~3 nm Cu prior to deposition of ~30 nm of Au, and annealing the film at 150 °C for ~45 min. The Cu-rich layer reduces the width of the space charge region, thus narrowing the barrier width sufficiently to allow efficient carrier tunneling to the Au; the result is a pseudo-ohmic contact. Compared to the Au-only contact, the Cu/Au contact (Fig. 3a) improved the V_{OC} from 0.68 V to 0.79 V, and efficiency improved from 8.7% to 11.4%.

When the Cu deposition and interdiffusion was replaced by a ~1.0 μm thick FeS_2 NC layer at room temperature and 30 nm thick Au atop of it (green curve, Fig. 3a), performance of the device approached that of the Cu/Au contact. The hydrazine-treated FeS_2 NC back contact showed a V_{OC}=0.77 V, J_{SC}=21.7 mA cm^{-2}, and 10.6% efficiency. In contrast with the Cu/Au contact, the device was never heated following the $CdCl_2$ activation step. The fill factor did decrease, as is evident in Fig. 3a, in accord with a residual barrier and a slight increase in the series resistance at the maximum power point. The increase in the J_{SC} has been frequently observed for the FeS_2-NC contact, and tests are ongoing to confirm and understand the effect. One possible source of the increased J_{SC} is a reduced interfacial recombination velocity at the back contact. We have also considered the possibility of a systematic error in the device area, but integration of the spectral response at short-

Table 1
Average parameters for three sets of 15 sputtered CdTe solar cells, with each set based on a different back contact. Each tested device was defined by either a shadow mask (device area = 0.080 cm^2) in the case of the Au-only and Cu–Au contacts, or by mechanical or laser scribing (device area = 0.085 cm^2) in the case of the FeS_2-NC/Au contact.

Back contact	V_{OC} (V)	J_{SC} (mA cm^{-2})	Fill factor (%)	Efficiency (%)	Series resistance (Ω cm^2)
Au	0.65 ± 0.04	20.2 ± 0.9	59.3 ± 2.4	7.7 ± 0.8	7.7 ± 0.6
Cu/Au	0.79 ± 0.02	21.8 ± 0.7	65.4 ± 1.9	11.3 ± 0.9	5.4 ± 0.9
FeS_2-NC/Au	0.77 ± 0.01	22.4 ± 1.0	61.5 ± 1.0	10.6 ± 0.4	6.9 ± 0.4

circuit confirmed ~3% higher J_{SC} for FeS_2-NC back-contacted devices. Carrier collection efficiency of the sputtered devices was examined by external quantum efficiency (EQE) measurement (Fig. 3b). The Cu-containing device shows a slightly reduced response for wavelengths most strongly absorbed by the CdS, suggesting an increased recombination rate in the CdS. It can be seen that current collection from FeS_2-NC/Au back contact device is slightly higher than for the Cu/Au device, except near the long wavelength cutoff. Our initial analysis indicates the long wavelength response may fall slightly for the case of the FeS_2-NC back contact due to reduced reflection of photons with energies near the CdTe band gap energy, where CdTe is weakly absorbing.

We performed a light intensity dependence study of FeS_2-NC/Au and Cu/Au back contact devices. Linear behavior of J_{SC} vs. irradiance data up to 1 sun (Fig. S3) at room temperature, can be attributed to two factors. First, photo-generation increases linearly with increasing irradiance intensity, and second, non-geminate recombination (recombination of charge carriers generated by two different photons) at short-circuit conditions is negligible such that all separated charges can be extracted with a probability independent of photogenerated carrier concentration [59]. This fact is further supported by Fig. 4a, in which the intensity dependence of the fill factor is demonstrated. Fill factor increases toward lower excitation intensity, which is due to the decrease in resistive loss at the lower operating current corresponding to lower incident intensity. For the FeS_2-NC/Au back contact, the fill factor increases from ~62% at 100 mW cm^{-2} to ~69% at 20 mW cm^{-2} (Fig. 4a).

We compared the thermal stability of the FeS_2-NC/Au back contact device with that of the standard Cu/Au back contact. Following initial performance characterization at room temperature, the devices were heated to 100 °C for several hours in a N_2 environment. Over a 24 h period, the efficiency of the best cell with the FeS_2-NC/Au back contact decreased from 10.7% to 10.3%. All *J-V* tests were performed once the devices equilibrated to room temperature. During this 24 h time period, V_{OC} decreased by 2.8% though other parameters remained essentially unchanged (FF increased slightly). Fig. 4b shows performance of the FeS_2-NC/Au back contact device (sputtered CdTe) before and after thermal treatment. The statistics of the *J–V* parameters in this temperature dependent study, when FeS_2-NC/Au was used as back contact, are shown in Table S1 and the temperature dependent *J–V* characteristics for the Cu/Au, and Au-only back contact devices are shown in Fig. S4 (in S.I.). These initial stability tests indicate that the devices with FeS_2-NC/Au back contact show thermal stability comparable with that of devices using our standard laboratory Cu/Au back contact. Although the mechanism of Cu-diffusion-based degradation is well-established, for the Cu-free FeS_2 contact we speculate that degradation arises from either (a) the development of FeS phases deviating from the FeS_2 stoichiometry, yielding Fe-rich and/or S-rich interfaces, or (b) from an interfacial contact effect at the CdTe/FeS_2 or FeS_2/Au–possibly induced by differential thermal expansion.

We investigated the dependence of device performance on the FeS_2 NC thickness as a back contact, using CSS-deposited CdS/CdTe device structures [60]. The type of CdS/CdTe CSS depositions utilized in our studies showed a champion cell efficiency of 14.3%

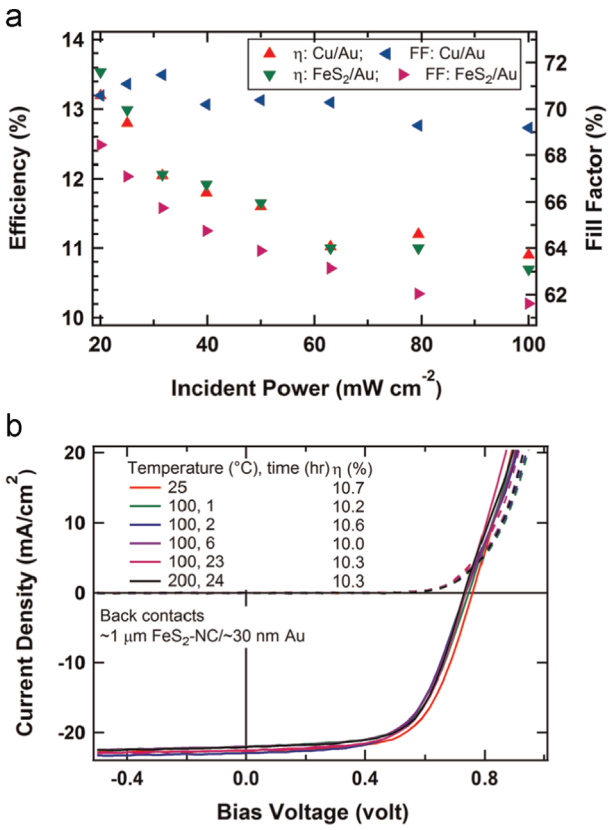

Fig. 4. (a) Comparison of the light intensity dependence on the efficiency and fill factor of sputtered CdS/CdTe devices when Cu/Au and FeS_2-NC/Au were used as the back contacts; (b) *J–V* curves of sputtered CdS/CdTe devices, with FeS_2-NC/Au back contacts, before and after heat treatment under N_2 atmosphere for 24 h.

under STC for the standard Cu/Au back contact. We studied the effect of replacing the Cu with varying thicknesses of FeS_2 NC layers (from 0.35 μm to 1.4 μm), fixing the other device architecture and processing parameters. As above, a ~30 nm Au layer was deposited following fabrication of the hydrazine-treated FeS_2-NC film. The performance parameters of these devices were compared with a standard device using Cu/Au as a back contact. Current density vs. voltage curves for all four device designs along with their performance parameters for the best cells are shown in Fig. 5. Detailed performance parameters and statistics are provided in Table S2 in S.I. Current density vs. voltage tests show that thin FeS_2 layers (0.35 μm) yield poor performance due to lower V_{OC}, perhaps due to an increased density of pinholes through which Au may contact the CdTe directly. The thickest FeS_2-NC film (1.4 μm) showed an increased effective series resistance and a slightly decreased V_{OC}. Comparatively low photo-conversion efficiency of the device using a back contact of 0.35 μm thick FeS_2 with 30 nm of Au is primarily due to the low V_{OC}; in contrast, the thickest FeS_2 contact layer showed a good V_{OC} but J_{SC} and FF were reduced, as was the overall device efficiency. Our measurements showed an optimal device performance for FeS_2 NC layer thickness of ~0.7 μm, with an efficiency ~13% below that of the champion Cu/

Au back contact device (the champion device resulted from separate studies, but under nominally identical processing conditions).

To determine whether hydrazine treatment alone affects the CdS/CdTe material and influences device performance, two standard solar cell device samples (~15 individual devices each) were prepared using sputtered CdS/CdTe, without the presence of the FeS_2 layer. Before back contact deposition, one of the devices was treated by soaking in 1 M hydrazine solution for two minutes followed by an ethanol rinse and drying in N_2. The Cu/Au back contact deposition was then completed using the normal procedure. Fig. S5 displays representative *J–V* characterizations of these completed devices. We observe statistically identical performance between the data sets, indicating that hydrazine alone does not measurably influence the PV properties of the CdTe. Although during FeS_2 NC deposition the hydrazine treatment likely does reach the CdTe (e.g., through pinholes following the first layer of NC FeS_2), the degree of contact is reduced with each subsequent drop-cast layer of FeS_2.

In order to understand the contact and device behavior, we have characterized the electrical properties of FeS_2 NC films using hot probe measurements as well as four point probe and Hall measurement methods [48]. All hot probe measurements indicated clearly that the films were p-type, in agreement with reports from other polycrystalline and NC-based FeS_2 films [8,10,61], indicating that the majority charge carriers in our pyrite films are holes. Four point probe measurement of untreated NC films revealed a typical sheet resistance of $\sim 10^5\ \Omega/\square$ and resistivity of ~100–200 Ω cm. For hydrazine treated films, sheet resistance decreased to $\sim 10^4\ \Omega/\square$ and resistivity to ~10–20 Ω cm. It is understood that Hall measurements made on polycrystalline films reveal the carrier concentration of the individual grains and the conductivity as determined by grain boundary scattering [62]. Our sheet resistance values measured by Hall effect and by four point probe generally agree quite well. The improved conductivity of the hydrazine treated films correlates with the removal of the surfactant molecules from the surface of the NCs which insulate neighboring NCs and inhibit efficient carrier transport. Though the overall FeS_2 NC stoichiometry is nearly ideal, we believe that the surfaces of the nanocubes are sulfur-rich and largely responsible for the p-type behavior we observe. The surface area to volume ratio is relatively high for these samples, and the significant surface-related contribution to the defect-based carrier density yields the near-degenerate p-type doping that supports formation of low-barrier contact to p-CdTe.

Comparing the performance of devices based on FeS_2 NC contacts prepared with and without hydrazine treatment reveals additional insights into the role played by the surfactant molecules, and the improvements resulting from their removal. During the synthesis of these NCs, TOPO controls the growth rate, influences the size and shape of the NCs, and caps the NC surface. The ~2 nm length of the TOPO molecules sheathe the NCs and maintain isolation between neighboring NCs within the film [63]. Cube-shaped FeS_2 NCs capped with TOPO molecules are displayed in Fig. 6a. As a strong reducing agent, hydrazine scavenges oxygen which breaks the linkage between the TOPO and the NC (Fig. S6). As TOPO is removed from the film, the NC films densify and the NC–NC electrical transport improves. Devices prepared with FeS_2 NC layers omitting hydrazine treatment exhibit dramatically different current–voltage behavior. Fig. 6b presents *J–V* curves for sputtered CdTe solar cells prepared with back contacts of untreated FeS_2-NC layers with Au. The untreated film shows a clear S-shape signature, indicative of a transport barrier formed at the back contact. Similar "S-kink" shapes have been previously observed under illumination in CIS and also in organic solar cells (OSCs) when a charge buildup occurs at one contact [64–66], and recent work has sought to explain and suppress the effect in OSCs [67]. Inflection points in the *J–V* curves observed in some organic solar cells are attributed to charge transport layers energetically misaligned to the energy levels of the active materials in planar heterojunction solar cells. In our case, the proposed charging behavior is attributed to the residual barrier at the CdTe/FeS_2-NC interface (possibly exacerbated by the low-mobility of the FeS_2 NC film) resulting in the S-kink behavior.

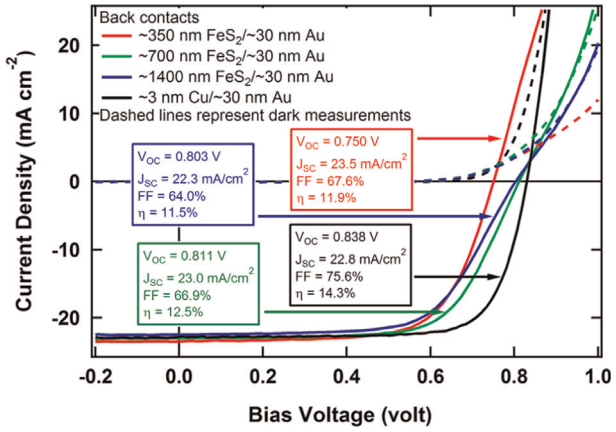

Fig. 5. *J–V* curves for CSS-deposited CdTe devices when the FeS_2-NC contact layer thickness was varied from 0.35 μm to 1.4 μm. Performance parameters for each device are shown in the boxes.

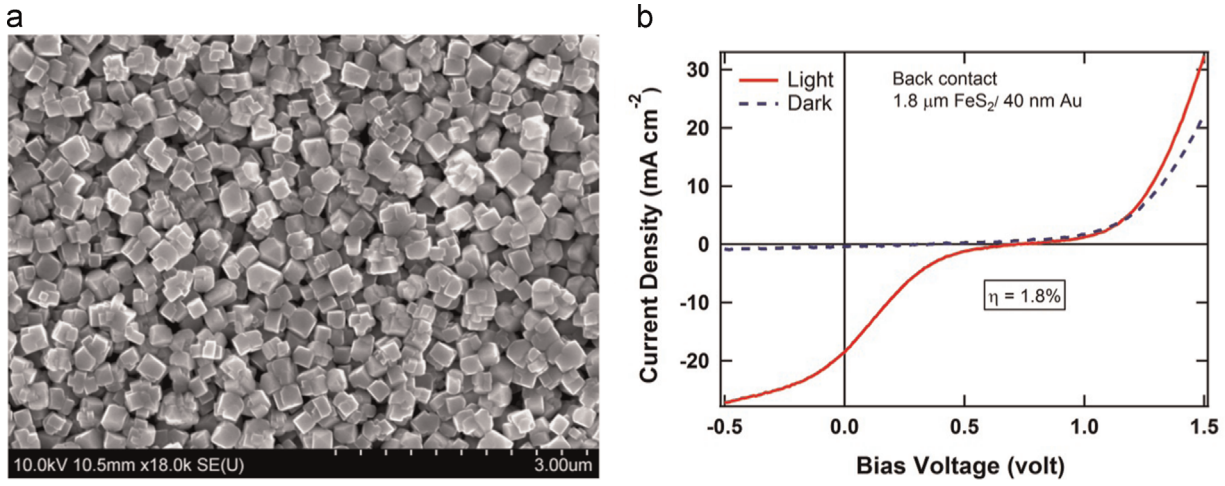

Fig. 6. (a) SEM image of FeS_2 NCs at 10 kV accelerating potential; (b) *J–V* curves when an untreated FeS_2-NC film was used as a back contact for sputtered CdTe solar cells.

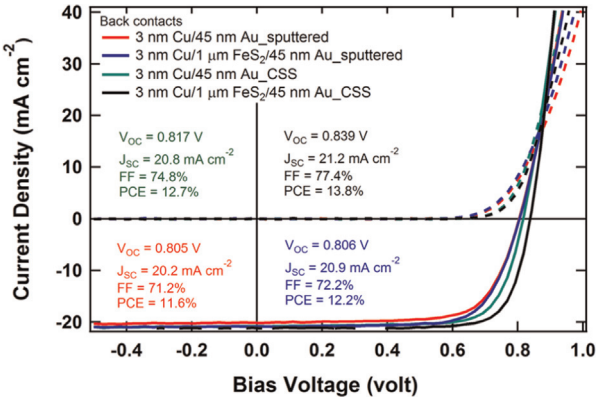

Fig. 7. Current density voltage characteristics of CdTe devices, when the back contact is deposited as a combination of Cu/FeS_2-NC/Au for both sputtered and CSS CdTe devices. The parameters shown in the graph are for the best cell.

We note that the S-kink shape also appears, albeit subtly, in the illuminated *J–V* curves for the two thickest FeS_2-NC contact devices in Fig. 5. The quantity d^2J/dV^2 dips briefly to negative values in the power generating quadrant for nearly all FeS_2-NC/Au back contact devices (Figs. S7 and S8).

Within the power-generating quadrant, electron–hole pairs photogenerated within the CdTe separate under the built-in field and move toward their respective electrodes. The TOPO-capped FeS_2 NC film presents a significant barrier to hole transport at the interface with CdTe, such that photogenerated carriers near the CdS/CdTe interface or within the CdTe layer experience impeded transport once reaching the FeS_2 NC layer. This is due to the insulating inter-NC surfactant layer which persists when the FeS_2-NC layer is untreated, or incompletely treated, with hydrazine. In such a case, holes may accumulate at the CdTe/FeS_2-NC interface and produce a barrier which is overcome only at sufficiently high forward bias for which the dark current dominates total current. Consequently, as the bias increases in the power-generating quadrant and the built-in field decreases, the device current drops due to the effective back contact diode established at the CdTe/FeS_2-NC interface. The hole transfer barrier and charge accumulation increase recombination and decrease current, resulting in an S-kink. For such devices to function optimally, one must sufficiently lower the effective resistance at the CdTe/FeS_2-NC interface through a deep valence band edge and a high free hole concentration; these conditions are achieved with the FeS_2 NC film after the hydrazine treatment.

We have also investigated the role played by Cu in an FeS_2-NC/Au back contact design: Two sets of devices were fabricated where three-layer back contacts were deposited: 3 nm Cu/1 μm FeS_2/45 nm Au. This experiment was done for both sputtered and CSS CdTe devices. In this case, as shown in Fig. 7, the presence of the FeS_2 NC layer improved the performance of the devices compared with that of the standard Cu/Au back contact devices (statistics of 20 cells in each case are provided in S.I.). The thin layer of Cu utilized in the standard CU/Au back contact improves performance by increasing the CdTe free hole concentration, one effect of which is a narrowing of the residual back barrier and improved hole tunneling efficiency. however, this does not completely make the barrier ohmic. When the FeS_2-NC layer is deposited onto is and the device is completed with Au, the performance of the device increases. Copper narrows the barrier width, and FeS_2 reduces the shunt resistance and increases V_{OC}, perhaps because the FeS_2 NC layer serves as a buffer layer with a relatively high work function. The device efficiency improves by ~5–9% when incorporating a FeS_2 NC layer between the Cu-treated CdTe and the Au external contact layer.

4. Conclusion

We have achieved a high degree of control over the crystallinity and stoichiometry of iron pyrite nanocubes, and recognition that the high work function of FeS_2 and the high free hole concentration of our FeS_2 NC films have enabled their implementation as a low-barrier back contact to CdTe within a Cu-free architecture. This work illustrates the application of FeS_2 NC as a low barrier electrical contact to thin film solar cells without the intentional preparation of a p+ highly-doped CdTe or $Cu_{2-x}Te$ layer that would serve to narrow any barrier width and facilitate tunneling. Our results show promise for the development of an iron-based contact material, and suggests the investigation of other related pyrites such as $FeTe_2$ and $FeSe_2$ as potential electronic materials relevant to the PV industry. Additional optimization of transport through the FeS_2 NC contact layer may further improve performance via removal of any mobility-induced resistance. The FeS_2 layer is easily prepared using a room-temperature and solution-based approach, and initial accelerated lifetime tests indicated stability comparable to that of the laboratory standard Cu/Au contact.

Acknowledgments

KPB, YY, NRP, and RJE were supported by the National Science Foundation's Sustainable Energy Pathways Program under Grant CHE-1230246; PK and RWC were supported by the DOE/NSF F-PACE Program (Contract DE-EE0005405). RRK, ABP, and MJH were supported by the Department of Energy under Award number DE-SC0006349 and by faculty start-up funds from the University of Toledo. KPB and RJE also gratefully acknowledge support from the United States Air Force Research Laboratory under Contracts FA9453-08-C-0172 and FA9453-11-C-0253. RJE acknowledges the support of start-up funds from the University of Toledo's College of Natural Sciences and Mathematics, and Wright Center for Photovoltaics Innovation and Commercialization.

Appendix A. Supplementary material

Supplementary data associated with this article can be found in the online version at http://dx.doi.org/10.1016/j.solmat.2015.03.032.

References

[1] A. Ennaoui, H. Tributsch, Iron sulphide solar cells, Sol. Cells 13 (1984) 197–200.
[2] A. Ennaoui, H. Tributsch, Energetic characterization of the photoactive FeS_2 (pyrite) interface, Sol. Energy Mater. 14 (1986) 461–474.
[3] A. Ennaoui, S. Fiechter, W. Jaegermann, H. Tributsch, Photoelectrochemistry of highly quantum efficient single-crystalline n-FeS_2 (Pyrite), J. Electrochem. Soc. 133 (1986) 97–106.
[4] A. Ennaoui, S. Fiechter, C. Pettenkofer, N. Alonso-Vante, K. Büker, M. Bronold, C. Höpfner, H. Tributsch, Iron disulfide for solar energy conversion, Sol. Energy Mater. Sol. Cells 29 (1993) 289–370.
[5] B. Rezig, H. Dahman, M. Kenzari, Iron pyrite FeS_2 for flexible solar cells, Renew. Energy 2 (1992) 125–128.
[6] K. Büker, N. Alonso-Vante, H. Tributsch, Photovoltaic output limitation of n-FeS_2 (pyrite) Schottky barriers: a temperature-dependent characterization, J. Appl. Phys. 72 (1992) 5721–5728.
[7] G. Chatzitheodorou, S. Fiechter, R. Könenkamp, M. Kunst, W. Jaegermann, H. Tributsch, Thin photoactive FeS_2 (pyrite) films, Mater. Res. Bull. 21 (1986) 1481–1487.
[8] Y. Bi, Y. Yuan, C.L. Exstrom, S.A. Darveau, J. Huang, Air stable photosensitive, phase pure iron pyrite nanocrystal thin films for photovoltaic application, Nano Lett. 11 (2011) 4953–4957.
[9] J. Puthussery, S. Seefeld, N. Berry, M. Gibbs, M. Law, Colloidal iron pyrite (FeS_2) nanocrystal inks for thin-film photovoltaics, J. Am. Chem. Soc. 133 (2010) 716–719.

[10] A. Kirkeminde, R. Scott, S. Ren, All inorganic iron pyrite nano-heterojunction solar cells, Nanoscale 4 (2012) 7649–7654.
[11] H.A. Macpherson, C.R. Stoldt, Iron pyrite nanocubes: size and shape considerations for photovoltaic application, ACS Nano 6 (2012) 8940–8949.
[12] A. Kirkeminde, B.A. Ruzicka, R. Wang, S. Puna, H. Zhao, S. Ren, Synthesis and optoelectronic properties of two-dimensional FeS_2 nanoplates, ACS Appl. Mater. Interfaces 4 (2012) 1174–1177.
[13] D.-Y. Wang, Y.-T. Jiang, C.-C. Lin, S.-S. Li, Y.-T. Wang, C.-C. Chen, C.-W. Chen, Solution-processable pyrite FeS_2 nanocrystals for the fabrication of heterojunction photodiodes with visible to NIR photodetection, Adv. Mater. 24 (2012) 3415–3420.
[14] J.M. Lucas, C.-C. Tuan, S.D. Lounis, D.K. Britt, R. Qiao, W. Yang, A. Lanzara, A.P. Alivisatos, Ligand-controlled colloidal synthesis and electronic structure characterization of cubic iron pyrite (FeS_2) nanocrystals, Chem. Mater. 25 (2013) 1615–1620.
[15] M. Gong, A. Kirkeminde, Y. Xie, R. Lu, J. Liu, J.Z. Wu, S. Ren, Iron pyrite (FeS_2) broad spectral and magnetically responsive photodetectors, Adv. Opt. Mater. 1 (2013) 78–83.
[16] A. Kirkeminde, S. Ren, Thermodynamic control of iron pyrite nanocrystal synthesis with high photoactivity and stability, J. Mater. Chem. A 1 (2013) 49–54.
[17] W. Ki, H.W. Hillhouse, Earth-abundant element photovoltaics directly from soluble precursors with high yield using a non-toxic solvent, Adv. Energy Mater. 1 (2011) 732–735.
[18] K. Woo, Y. Kim, J. Moon, A non-toxic, solution-processed, earth abundant absorbing layer for thin-film solar cells, Energy Environ. Sci. 5 (2012) 5340–5345.
[19] K. Hui-Seon, L. Chang-Ryul, I. Jeong-Hyeok, L. Ki-Beom, M. Thomas, M. Arianna, M. Soo-Jin, H.-B. Robin, Y. Jun-Ho, E.M. Jacques, G. Michael, P. Nam-Gyu, Lead iodide perovskite sensitized all-solid-state submicron thin film mesoscopic solar cell with efficiency exceeding 9%, Sci. Rep. 2 (2012) 1–7.
[20] K.P. Bhandari, P.J. Roland, H. Mahabaduge, N.O. Haugen, C.R. Grice, S. Jeong, T. Dykstra, J. Gao, R.J. Ellingson, Thin film solar cells based on the heterojunction of colloidal PbS quantum dots with CdS, Sol. Energy Mater. Sol. Cells 117 (2013) 476–482.
[21] A.H. Ip, S.M. Thon, S. Hoogland, O. Voznyy, D. Zhitomirsky, R. Debnath, L. Levina, L.R. Rollny, G.H. Carey, A. Fischer, K.W. Kemp, I.J. Kramer, Z. Ning, A.J. Labelle, K.W. Chou, A. Amassian, E.H. Sargent, Hybrid passivated colloidal quantum dot solids, Nat. Nanotechnol. 7 (2012) 577–582.
[22] L. Yu, S. Lany, R. Kykyneshi, V. Jieratum, R. Ravichandran, B. Pelatt, E. Altschul, H.A.S. Platt, J.F. Wager, D.A. Keszler, A. Zunger, Iron chalcogenide photovoltaic absorbers, Adv. Energy Mater. 1 (2011) 748–753.
[23] K. Ellmer, C. Höpfner, On the stoichiometry of the semiconductor pyrite (FeS_2), Philos. Mag. A 75 (1997) 1129–1151.
[24] D. Rickard, G.W. Luther, Chemistry of iron sulfides, Chem. Rev. 107 (2007) 514–562.
[25] First solar hits cost reduction milestone. ⟨http://www.pv-tech.org/news/has_first_solar_retaken_the_lowest_cost_pv_manufacturer_mantle⟩, 2013.
[26] R.K. Swank, Surface properties of II–VI compounds, Phys. Rev. 153 (1967) 844–849.
[27] J. Freeouf, J. Woodall, Schottky barriers: an effective work function model, Appl. Phys. Lett. 39 (1981) 727–729.
[28] U. Avachat, Development of Transparent and Conducting Back Contacts on CdS/CdTe Solar Cells for Photoelectrochemical Application, University of Central Florida Orlando, Florida, 2005.
[29] E. Janik, R. Triboulet, Ohmic contacts to p-type cadmium telluride and cadmium mercury telluride, J. Phys. D: Appl. Phys. 16 (1983) 2333.
[30] C.R. Corwine, A.O. Pudov, M. Gloeckler, S.H. Demtsu, J.R. Sites, Copper inclusion and migration from the back contact in CdTe solar cells, Sol. Energy Mater. Sol. Cells 82 (2004) 481–489.
[31] T.J. Berniard, D.S. Albin, B. To, J.W. Pankow, M. Young, S.E. Asher, Effects of Cu at the device junction on the properties of CdTe/CdS photovoltaic cells, J. Vacuum Sci. Technol. B 22 (2004) 2423–2428.
[32] K.D. Dobson, I. Visoly-Fisher, G. Hodes, D. Cahen, Stability of CdTe/CdS thin-film solar cells, Sol. Energy Mater. Sol. Cells 62 (2000) 295–325.
[33] H. Dahman, M. Khalifa, M. Brunel, B. Rezig, Iron pyrite films prepared by sulfur vapor transport, Thin Solid Films 280 (1996) 56–60.
[34] S. Fiechter, M. Birkholz, A. Hartmann, P. Dulski, M. Giersig, H. Tributsch, R.J.D. Tilley, The microstructure and stoichiometry of pyrite FeS_{2-x}, J. Mater. Res. 7 (1992) 1829–1838.
[35] S. Krum, First Solar achieves efficiency, durability milestones, Acquire Media, First Solar Inc. ⟨http://invetorirtolar.co/releasedetail.cfm?ReleaseD=895118⟩, 2015.
[36] M.A. Islam, M.S. Hossain, M.M. Aliyu, M.R. Karim, T. Razykov, K. Sopian, N. Amin, Effect of $CdCl_2$ treatment on structural and electronic property of CdTe thin films deposited by magnetron sputtering, Thin Solid Films 546 (2013) 367–374.
[37] A.J. Al-Douri, F.Y. Al-Shakily, A.A. Alnajjar, M.F.A. Alias, The role of dopant concentration on conductivity and mobility of CdTe thin films, Adv. Condens. Matter Phys. 2011 (2011).
[38] S. Trigwell, M. Mazumder, R. Pellissier, Tribocharging in electrostatic beneficiation of coal: effects of surface composition on work function as measured by x-ray photoelectron spectroscopy and ultraviolet photoelectron spectroscopy in air, J. Vacuum Sci. Technol. A 19 (2001) 1454–1459.
[39] E.V. Buzaneva, P. Scharff, Frontiers of multifunctional nanosystems, IOS Press, Amsterdam, Kluwer Academic Publishers in conjunction with the NATO Scientific Affairs Division, 2002.
[40] A. Baldereschi, C. Fall, Ab Initio Study of the Work Functions of Elemental Metal Crystals, Département de Physique, École Polytechnique Fédérale de Lausanne, Switzerland, 1999.
[41] B. de Boer, A. Hadipour, M.M. Mandoc, T. van Woudenbergh, P.W.M. Blom, Tuning of metal work functions with self-assembled monolayers, Adv. Mater. 17 (2005) 621–625.
[42] S.G. Kumar, K.K. Rao, Physics and chemistry of CdTe/CdS thin film heterojunction photovoltaic devices: fundamental and critical aspects, Energy Environ. Sci. 7 (2014) 45–102.
[43] J. Fritsche, D. Kraft, A. Thißen, T. Mayer, A. Klein, W. Jaegermann, Band energy diagram of CdTe thin film solar cells, Thin Solid Films 403 (2002) 252–257.
[44] D. Albin, D. Levi, S. Asher, A. Balcioglu, R. Dhere, J. Hiltner, Precontact surface chemistry effects on CdS/CdTe solar cell performance and stability, in: Proceedings of the IEEE 29th Photovoltaic Specialists Conference (PVSC), September 15–22, Anchorage, AK, 2000, pp. 583–586.
[45] J. Liang, H. Bi, D. Wan, F. Huang, Novel Cu nanowires/graphene as the back contact for CdTe solar cells, Adv. Funct. Mater. 22 (2012) 1267–1271.
[46] T. Lin, F. Huang, J. Liang, Y. Wang, A facile preparation route for boron-doped graphene, and its CdTe solar cell application, Energy Environ. Sci. 4 (2011) 862–865.
[47] A.B. Phillips, R.R. Khanal, Z. Song, R.M. Zartman, J.L. DeWitt, J.M. Stone, P.J. Roland, V.V. Plotnikov, C.W. Carter, J.M. Stayancho, R.J. Ellingson, A. D. Compaan, M.J. Heben, Wiring-up carbon single wall nanotubes to polycrystalline inorganic semiconductor thin films: low-barrier, copper-free back contact to CdTe solar cells, Nano Lett. 13 (2013) 5224–5232.
[48] K.P. Bhandari, P.J. Roland, T. Kinner, Y. Cao, H. Choi, S. Jeong, R.J. Ellingson, Analysis and characterization of iron pyrite nanocrystals and nanocrystalline thin films derived from bromide anion synthesis, J. Mater. Chem. A 3 (2015) 6853–6861.
[49] J.M. Luther, M. Law, M.C. Beard, Q. Song, M.O. Reese, R.J. Ellingson, A.J. Nozik, Schottky solar cells based on colloidal nanocrystal films, Nano Lett. 8 (2008) 3488–3492.
[50] J. Tang, X. Wang, L. Brzozowski, D.A.R. Barkhouse, R. Debnath, L. Levina, E.H. Sargent, Schottky quantum dot solar cells stable in air under solar illumination, Adv. Mater. 22 (2010) 1398–1402.
[51] K.P. Bhandari, P.J. Roland, G. Jianbo, R.J. Ellingson, Bandgap, window layer thickness, and light soaking effects on PbS quantum dot solar cells, in: Proceedings of the IEEE 39th Photovoltaic Specialists Conference (PVSC), June 16–21, Tampa Convention Center, Tampa, FL, USA, 2013, pp. 0258–0263.
[52] P. Koirala, D. Attygalle, P. Aryal, P. Pradhan, J. Chen, S. Marsillac, A.S. Ferlauto, N.J. Podraza, R.W. Collins, Real time spectroscopic ellipsometry for analysis and control of thin film polycrystalline semiconductor deposition in photovoltaics, Thin Solid Films 571 (2014) 442–446.
[53] V. Plotnikov, X. Liu, N. Paudel, D. Kwon, K.A. Wieland, A.D. Compaan, Thin-film CdTe cells: reducing the CdTe, Thin Solid Films 519 (2011) 7134–7137.
[54] A. Bosio, N. Romeo, S. Mazzamuto, V. Canevari, Polycrystalline CdTe thin films for photovoltaic applications, Prog. Cryst. Growth Charact. Mater. 52 (2006) 247–279.
[55] K.V. Krishna, V. Dutta, Effect of in situ $CdCl_2$ treatment on spray deposited CdTe/CdS heterostructure, J. Appl. Phys. 96 (2004) 3962–3971.
[56] K. Durose, P.R. Edwards, D.P. Halliday, Materials aspects of CdTe/CdS solar cells, J. Cryst. Growth 197 (1999) 733–742.
[57] S. Demtsu, J. Sites, Effect of back-contact barrier on thin-film CdTe solar cells, Thin Solid Films 510 (2006) 320–324.
[58] A. Niemegeers, M. Burgelman, Effects of the Au/CdTe back contact on IV and CV characteristics of Au/CdTe/CdS/TCO solar cells, J. Appl. Phys. 81 (1997) 2881–2886.
[59] R. Mauer, I.A. Howard, F. Laquai, Effect of nongeminate recombination on fill factor in polythiophene/methanofullerene organic solar cells, J. Phys. Chem. Lett. 1 (2010) 3500–3505.
[60] N.R. Paudel, Y. Yan, Fabrication and characterization of high-efficiency CdTe-based thin-film solar cells on commercial SnO_2:F-coated soda-lime glass substrates, Thin Solid Films 549 (2013) 30–35.
[61] G. Golan, A. Axelevitch, B. Gorenstein, V. Manevych, Hot-probe method for evaluation of impurities concentration in semiconductors, Microelectron. J. 37 (2006) 910–915.
[62] R.H. Bube, Interpretation of Hall and Photo-Hall effects in inhomogeneous materials, Appl. Phys. Lett. 13 (1968) 136–139.
[63] H. Graaf, M. Vieluf, Cv. Borczyskowski, Selective binding of dye molecules and CdSe nanocrystals on nanostructures generated by AFM lithography of silicon surfaces, Nanotechnology 18 (2007) 265306.
[64] I.L. Eisgruber, J.E. Granata, J.R. Sites, J. Hou, J. Kessler, Blue-photon modification of nonstandard diode barrier in $CuInSe_2$ solar cells, Sol. Energy Mater. Sol. Cells 53 (1998) 367–377.
[65] J.C. Wang, X.C. Ren, S.Q. Shi, C.W. Leung, P.K.L. Chan, Charge accumulation induced S-shape *J–V* curves in bilayer heterojunction organic solar cells, Org. Electron. 12 (2011) 880–885.
[66] W. Tress, S. Corvers, K. Leo, M. Riede, Investigation of driving forces for charge extraction in organic solar cells: transient photocurrent measurements on solar cells showing S-shaped current–voltage characteristics, Adv. Energy Mater. 3 (2013) 873–880.
[67] O. Tatsuya, H. Kenji, Attempt to suppress S-shaped kink in current–voltage characteristics in organic solar cells, Jpn. J. Appl. Phys. 52 (2013) 011601.